OPEN ACCESS Freely available online

PLOS ONE

Non Destructive Characterization of Cortical Bone Micro-Damage by Nonlinear Resonant Ultrasound Spectroscopy

Sylvain Haupert[1]*, Sandra Guérard[2], Françoise Peyrin[3,4], David Mitton[5], Pascal Laugier[1]

1 UPMC Univ Paris 06, CNRS UMR7623, Laboratoire d'Imagerie Paramétrique, Paris, France, **2** Arts et Métiers ParisTech, LBM, Paris, France, **3** CREATIS, INSERM U1044, CNRS 5220, INSA Lyon, Université Lyon 1, Lyon, France, **4** European Synchrotron Radiation Facility, Grenoble, France, **5** Université de Lyon, IFSTTAR, LBMC, UMR_T 9406, Université Lyon 1, Lyon, France

Abstract

The objective of the study was to evaluate the ability of a nonlinear ultrasound technique, the so-called nonlinear resonant ultrasound spectroscopy (NRUS) technique, for detecting early microdamage accumulation in cortical bone induced by four-point bending fatigue. Small parallelepiped beam-shaped human cortical bone specimens were subjected to cyclic four-point bending fatigue in several steps. The specimens were prepared to control damage localization during four-point bending fatigue cycling and to unambiguously identify resonant modes for NRUS measurements. NRUS measurements were achieved to follow the evolution of the nonlinear hysteretic elastic behavior during fatigue-induced damage. After each fatigue step, a small number of specimens was removed from the protocol and set apart to quantitatively assess the microcrack number density and length using synchrotron radiation micro-computed tomography (SR-μCT). The results showed a significant effect of damage steps on the nonlinear hysteretic elastic behavior. No significant change in the overall length of microcracks was observed in damaged regions compared to the load-free control regions. Only an increased number of shortest microcracks, those in the lowest quartile, was noticed. This was suggestive of newly formed microcracks during the early phases of damage accumulation. The variation of nonlinear hysteretic elastic behavior was significantly correlated to the variation of the density of short microcracks. Our results suggest that the nonlinear hysteretic elastic behavior is sensitive to early bone microdamage. Therefore NRUS technique can be used to monitor fatigue microdamage progression in *in vitro* experiments.

Citation: Haupert S, Guérard S, Peyrin F, Mitton D, Laugier P (2014) Non Destructive Characterization of Cortical Bone Micro-Damage by Nonlinear Resonant Ultrasound Spectroscopy. PLoS ONE 9(1): e83599. doi:10.1371/journal.pone.0083599

Editor: Ryan K. Roeder, University of Notre Dame, United States of America

Received June 21, 2013; **Accepted** November 5, 2013; **Published** January 2, 2014

Funding: This research was supported by the Agence Nationale pour la Recherche (ANR), France (Grant BONUS_07BLAN0197). The funders had no role in study design, data collection and analysis, decision to publish, or preparation of the manuscript.

Competing Interests: The authors have declared that no competing interests exist.

* E-mail: sylvain.haupert@upmc.fr

Introduction

Among various bone quality factor, bone microdamage is certainly the less understood, as *in vivo* microcracks detection is still challenging. Bone microdamage is a natural phenomenon caused by daily loading [1]. Microdamage manifests as linear microcracks and diffuse damage in cortical bone [2,3]. The density of linear microcrack increases significantly with age in cortical bone [2,4–6]. While microdamage is of little consequence under normal bone self-repair capability [7], microdamage accumulation following impaired repair capabilities caused by disease, age or drug absorption [8–10] is suspected to reduce bone biomechanical competence, including toughness [11,12], stiffness [11–16] and ultimate load [11,17]. Such alterations may lead ultimately to an increase in fracture risk [6]. Histomorphometry is the current gold standard to characterize microdamage *in vitro* [2,14]. However, quantitative assessment of microcracks with histomorphometry entails serial sectioning and observer intervention, which is usually time consuming. Moreover, as microcracks are relatively scarce in bone 2-D cross-sections, the statistical validity remains challenging [18].

Recently, synchrotron radiation micro-computed tomography (SR-μCT) enabled the 3-D assessment of microcracks at a micro-scale resolution [19–22]. These techniques are inherently destructive and cannot be used to study microdamage *in vivo*.

Several measurement modalities, including positron emission tomography (PET) [23,24], nuclear magnetic resonance NMR T2 relaxation time [25] and nonlinear ultrasound [26,27] are currently explored to non destructively assess microdamage in living bones.

Quantitative ultrasound is widely used to assess skeletal status [28]. However, the linear elastic (speed of sound) and dissipative (attenuation) parameters derived in quantitative ultrasound are not sensitive to damage [29–32]. Contrary to linear acoustics, in the framework of nonlinear acoustics, the propagation velocity and the attenuation (or dissipation) of acoustic waves are amplitude dependent. Those peculiarities give rise to various phenomena called nonlinear acoustical effects. Damaged materials have proved to exhibit a characteristic nonlinear behavior that can be used to infer material mechanical integrity. Elastic nonlinear parameters derived from dynamic wave studies were found to be far more sensitive than their linear counterparts to damage in a

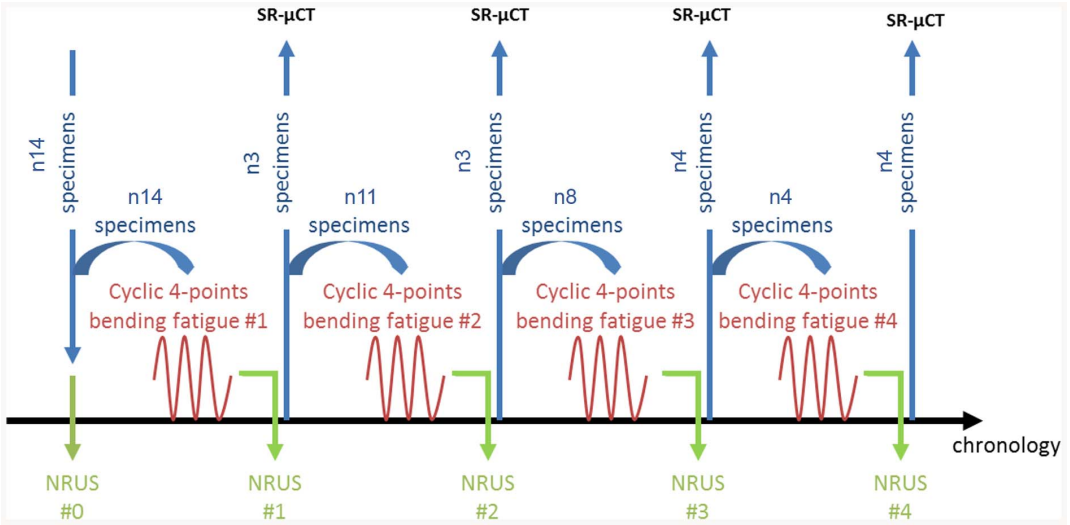

Figure 1. Diagram illustrating the experimental protocol.
doi:10.1371/journal.pone.0083599.g001

variety of materials [33,34]. This has recently motivated several research groups to adapt ultrasound-based nonlinear dynamic elastic testing methods to assess the level of microdamage in cortical or cancellous bone using different techniques. These include nonlinear ultrasonic resonant spectroscopy (NRUS) [35–37], dynamic acousto-elasticity testing (DAET) [38–40], harmonic generation [26,27] and nonlinear wave modulation spectroscopy [41,42]. The advantage of these nonlinear techniques is that they are inherently non destructive and can therefore potentially be implemented *in vivo* [26,27].

In previous NRUS studies, our group has reported that, under resonance conditions, the resonance frequency of damaged femoral diaphysis was down shifted with increasing vibration amplitude. We found a correlation of progressive fatigue of human bone samples to their nonlinear dynamical response [35–37]. Such an effect can be interpreted as a softening of the material in presence of cracks when the wave amplitude increases gradually (i.e., the modulus of the material decreases with dynamical forcing). This softening effect rises as the elastic non linearity (i.e., the level of damage) of the material increases [43]. With the possibility to non-invasively evaluate nonlinear properties assumed to be related to microdamage accumulation, NRUS is an attractive technique to evaluate microdamage in bone. In the above mentioned NRUS studies, nonlinear ultrasonic measurements were not validated by histology nor by high resolution µCT. The measured nonlinear elastic properties could not be correlated to microdamage characteristics. Therefore the goal of this study was to assess the relationships between the nonlinear elastic parameter and microdamage characteristics on human cortical bone specimens subjected to fatigue loading with a specific focus on assessment of the sensitivity of the technique to early phase of damage accumulation.

Materials and Methods

Specimen preparation and measuring protocol

Small parallelepiped beam-shaped human cortical bone specimens were subjected to cyclic four-point bending fatigue in several steps. The specimens were prepared to control damage localization during four-point bending fatigue cycling and to unambiguously identify resonant modes for NRUS measurements.

Fourteen human cortical bone specimens were prepared from the femoral mid-diaphysis of four female donors (78, 80, 98, 98 years old). Ethical approval for the collection of samples was granted by the Human Ethics Committee of the Centre du don des Corps at the University Paris Descartes (Paris, France). The tissue donors or their legal guardians provided informed written consent to give their tissue for investigation, in accord with legal clauses stated in the French Code of Public Health. The specimens were wet machined (Isomet 4000, Buehler GmbH, Düsseldorf, Germany) as parallelepiped beams (50*4*2 mm), defatted [44] and stored at -20°C until experiments.

Apparent dry density (ρ_{dry}) was evaluated by measuring the specimen volume and weight. Bone specimens were dried at 37°C during one night in a climate chamber (Memmert GmbH HCP 108, Schwabach, Germany) at relative humidity 15% in the presence of desiccators. Drying and rewetting procedure does not affect bone properties as the collagen molecular structure remains intact [45,46].

The procedure for the NRUS and mechanical studies began with the initial NRUS measurements for all specimens to determine the initial nonlinearity of the material. The specimens were then taken through a damage step, consisting of cyclic four-point bending as described below, during which mechanical parameters were determined. NRUS measurements were repeated after each cycling session. Four damage steps were achieved. After each damage step, three or four specimens were removed for future 3-D SR-µCT investigations of microdamage characteristics. The measurement protocol is illustrated in Fig. 1.

NRUS measurements

The principles of NRUS measurements have been extensively described elsewhere [43]. Briefly, a piezoceramic emitter (Fuji Ceramics Corporation, Yamamiya, Japan) glued on a backload (i.e. a heavy mass compared to the specimen) was bonded at one end of the specimens to ensure free-fix boundary conditions for NRUS measurements (Fig. 2). Each specimen was excited by a swept-sine (M2i.6012, Spectrum GmbH, Grosshansdorf, Germany) encompassing the first resonant modes of the cortical beam (assumed to be pure compression modes under asymmetric loading conditions). The dynamic strain amplitude ε was calculated from the longitudinal particle displacement U at one

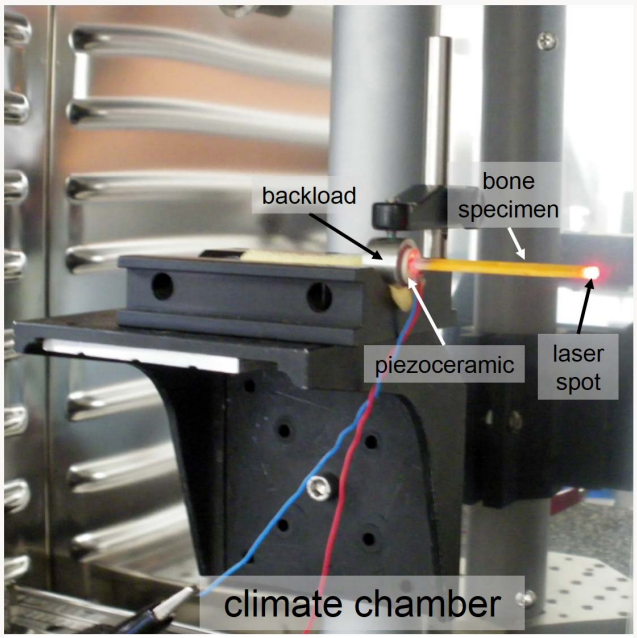

Figure 2. NRUS experimental setup. Bone specimen bonded on a piezoceramic emitter is placed in a climate chamber.
doi:10.1371/journal.pone.0083599.g002

end of the sample measured by a laser vibrometer (LSV 1MHz, SIOS, Ilmenau, Germany):

$$\varepsilon = \frac{\delta U}{\delta x} = U * k = \frac{U * 2\pi}{4L} \quad (1)$$

where k is the wave number and L is the specimen length. The resonance peak frequency f of the first compression mode was derived for each voltage drive level from the strain amplitude measured as a function of frequency at the corresponding excitation level. From the resonance peak data, the nonlinear parameter α_f can be calculated using the following equation [43,47]:

$$\frac{f - f_0}{f_0} = \frac{\Delta f}{f_0} = \frac{\alpha_f}{2}\Delta\varepsilon \quad (2)$$

where f is the resonance frequency at increased strain level and f_0 its corresponding value at the lowest drive amplitude [47]. Eq. 2 expresses that the frequency shift Δf is proportional to the peak strain amplitude $\Delta\varepsilon$ via the nonlinear elastic α_f parameter. This parameter, so-called nonlinear hysteretic elastic parameter, is typical of nonlinearities that appear for strains above approximately 10^{-5} [47] in damaged materials. It conveys information about the amount of hysteretic nonlinearity directly linked to damage accumulation in a material.

The widely used NRUS measurement protocol [43] was optimized to achieve high sensitivity. The measurement of the reference resonance frequency f_0 used to compute α_f was repeated before each excitation level. In doing so, the measurements become less affected by changes in environmental conditions such as temperature and yields more precise and stable α_f estimates [48].

During the NRUS measurements, specimens were kept at fixed temperature (37°C ±0.1°C) and relative humidity (15%±5%) into a climate chamber (Fig. 2)

Biomechanical testing

The piezoceramic emitter attached to the specimen for NRUS measurements was removed and the specimen was rehydrated during 48 hours before each mechanical testing. All specimens were progressively damaged by cyclic four-point bending at 2 Hz under load control in a saline solution at 37°C (±1°C) using a hydraulic testing machine (INSTRON, 8802, High Wycombe, England) with a 1 kN loading cell (accuracy 0.5%) and the internal displacement transducer (accuracy 1%). The specific four-point bending assembly composed of 6.35 mm diameter roller-bearings with a 40 mm outer span and a pivoting 20 mm inner span minimizes the formation of grooves under the rollers [49,50]. In this configuration, damage is expected to occur specifically in the mid region of the sample [12], while the distal regions remaining intact may be used as control. Initial Young's modulus was determined during pre-cycling after 20 cycles by measuring the slope of the linear portion of the last load-displacement curve.

From the initial Young's modulus, the load (*Fmax*) corresponding to 5000με (i.e. an initial strain rate of 20000με/s) at the mid-span was computed for all specimens [12]. The four-point bending fatigue was then applied between -10N and –*Fmax*. During the cycling session, the load and displacement curves were recorded to extract the linear elastic beam theory (LEBT) modulus (E_{LEBT}) as defined by Landrigan [51]. E_{LEBT} is a combination of elastic (secant modulus) and plastic (residual strain) biomechanical parameters. After each damage step, the E_{LEBT} modulus is normalized by the initial value measured for the first loading cycle of the first damage step. E_{LEBT} has been shown to decrease as bone microdamage accumulates [15,16,53]. The progressive damage was performed in four steps (one step = one cycling session), each step was defined by multi-criteria: 10% decrease of the E_{LEBT} or pre-determined number of cycles (= 6000) or anomalous E_{LEBT} decreasing speed. This multi-criteria definition of each step was chosen to achieve progressive damage accumulation and to avoid specimen failure before the end of the fourth step.

3-D synchrotron radiation μCT (SR-μCT)

At the end of each step, a subset of 3 or 4 bone specimens was measured by SR-μCT at the European Synchrotron Radiation Facility in Grenoble, France. Two different reconstructed volumes of interest (VOI) were investigated. VOI1, located in the load-free region at one distal end of the sample, outside of the roller-support, was assumed to be free of damage (except for pre-existing initial pre-fatigue damage). VOI2, located in the central portion of the beam, is the region where most microdamage was assumed to accumulate during mechanical fatigue. The photon energy was 25 KeV and the size of the VOI was $2.8\times2.8\times1.96 mm^3$ with a voxel size of 1.4 μm^3. A set of 2500 projections were acquired at an angular step of 0.144°. The $2048\times2048\times1400$ 3D images were reconstructed using a filtered back projection algorithm and the contrast was linearly rescaled to an 8-bits dynamic to save memory storage. For microdamage characterization, the size of the investigated volume of both VOIs was reduced to $2.2\times2.0\times1.96$ mm^3.

Microdamage is generally characterized on transverse or longitudinal 2-D sections by conventional or epifluorescence microscopy [12,14]. In this study, microdamage characteristics were quantitatively assessed in cortical bone volumes reconstructed from SR-μCT data. To this end, each VOI was sampled by eleven 2-D transverse cross-sections regularly spaced with an

interval of 180µm (Fig. 3). Each cross-section was obtained by averaging a stack of 18 adjacent 1.4µm-thick slices in order to achieve transverse cross-section images with a depth of field of 25 µm equivalent to that achieved with epifluorescence microscopy. The averaging process has also the advantage to decrease the noise level and to improve to contrast between the microcracks and the bone matrix.

The surface microcrack density (Cr.Dn [#.mm^2]) and microcrack length (Cr.Le [µm]) were measured using the software ImageJ (NIH, USA) with the plugin NeuronJ [52]. The bone surface was computed as the total area of bone section, including the pores (Haversian and Volkmann canals, and resorption cavities) as it is reported in the literature [8,54]. The pores appeared as dark pixels and were clearly evidenced as one peak of the bimodal gray level histograms of the image. Thus they could easily be separated from bone tissue using a thresholding method to keep only low grey level pixels, with a threshold set to 100 (arbitrary unit) in the range [0–255] according to the histogram. The porosity value corresponds to the number of segmented pixels (pores) over the total surface of cortical bone including pores (in pixels).

Microcracks characteristics were determined first by including all microcracks. In a second step, microcracks fully embedded within the bone volume were processed separately from microcracks leading to the surface as they are mainly artifactual microcracks formed during the preparation process [14,53,55].

Data analysis

Matlab 7.8 with statistics toolbox 7.6 (Mathworks, Natick, MA, USA) was used for statistical analyses. A non-parametric one-way analysis of variance (ANOVA) dedicated to repeated measurements (Friedman Test) followed by post hoc multiple comparison (Nemenyi test) was applied to test whether the levels of nonlinear elasticity achieved at each steps of the fatigue protocol were statistically significantly different. This analysis was performed on two subsets of the total set of specimens (N = 14). Group 1 (N = 8) includes all specimens having undergone the first three damage steps and Group 2 (N = 4) includes all specimens having undergone all the four damage steps. The effect of fatigue loading on microdamage characteristics (Cr.Dn and Cr.Le) in the control region and the damaged region was investigated with a non-parametric Wilcoxon signed rank test for all specimens (N = 14). The relationship of the nonlinear elastic parameter α_f with microdamage characteristics was obtained by a Spearman correlation test taking into account all specimens (N = 14) as well as after removing the outlier (N = 13). P-values less than 0.05 were considered significant.

Results

Individual results for mechanical and NRUS testing are presented in Table 1. In Table 2, we report only the microdamage characteristics for fully embedded microcracks as the results were similar when all microcracks were included in the analysis or after excluding those leading to the specimen surface.

Biomechanical testing

The variability of E_{LEBT} has been assessed on five dedicated specimens that were not included in the protocol. They went through 20 cycles (after system stabilization) of four-point bending test. The process was repeated 6 times with repositioning. The

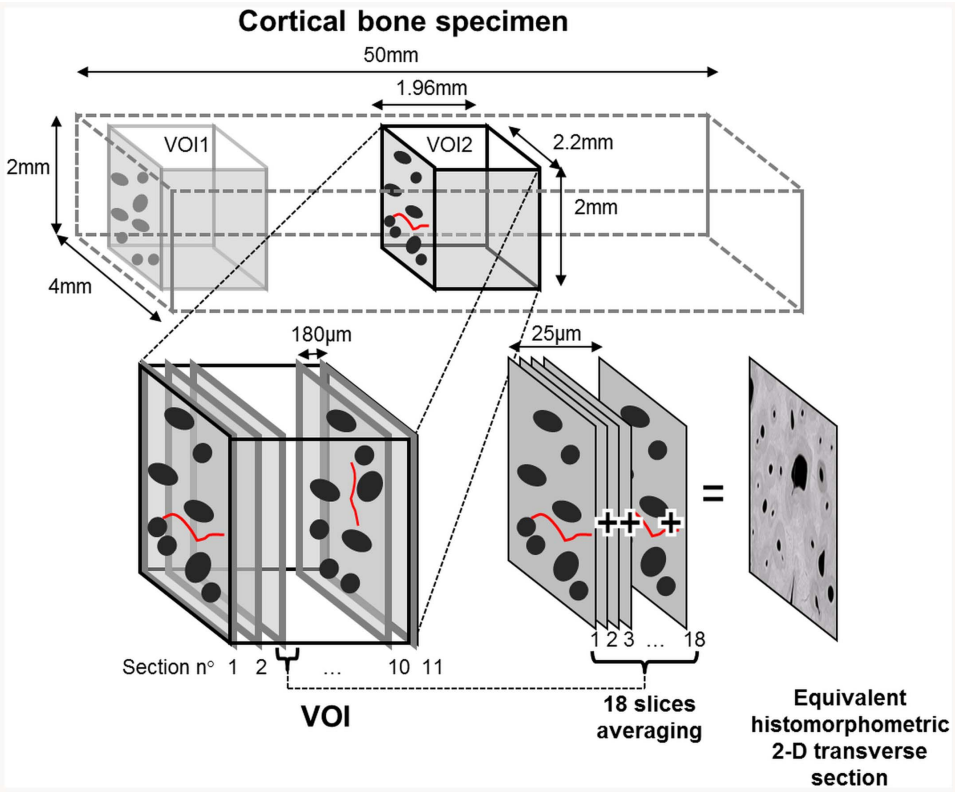

Figure 3. Diagram illustrating the process leading to an equivalent histomorphometric 2-D transverse cross-section image from 3-D reconstructed bone volumes acquired by SR-µCT.
doi:10.1371/journal.pone.0083599.g003

Table 1. Characteristics of the human cortical bone specimens: density (ρ_{dry}), initial mechanical modulus LEBT (E_{LEBT}), number of damage steps, number of cycles, initial, intermediate and final nonlinear elastic parameters (α_f).

	Architectural		*Mechanical (wet)*			*Nonlinear ultrasonic parameters (dry)*				
Specimens	ρ_{dry} [g/cm3]	Porosity [%]	initial E_{LEBT} [KPa]	final E_{LEBT} [KPa]	*Total num of cycles*	α_f initial	α_f step 1	α_f step 2	α_f step 3	α_f step 4
#1	1753	11.4	15215	nm	155	−6	−6.4			
#2	1897	13.2	17069	nm	120	−4.8	−4.7			
#3	1870	6.3	17294	16027	906	−15.5	-15.3			
#4	1865	10.3	17382	12583	2100	−4.6	−5.9	−5.8		
#5	1353	26.5	9344	nm	175	−4.7	−6.4	-12.8		
#6	1854	12.4	15654	9799	1991	−4.4	−9.8	-15.4		
#7	1887	7.3	15722	11619	1788	−6	−9.7	-12.8	-16.2	
#8	2005	5.6	21857	14760	6226	−6.2	−6	−6.1	−6.5	
#9	1904	9.8	16598	14133	9220	−4.7	−5.7	−6.4	−7.1	
#10	1893	9.4	16296	11980	3275	−4.5	−4.6	−4.2	−6.2	
#11	1864	14.2	16055	9289	4221	−5	−4.4	−5	−5.9	−6
#12	1714	13.1	13470	7901	13826	−5.1	−6	−6.1	−6.5	−6.3
#13	1684	12.6	11876	7054	3616	−4.3	−4.9	−6.2	−6.1	−7.3
#14	1821	16.3	14406	11177	14396	−4.8	−5.2	−5.9	−6.6	-10.7
Mean	**1812**	**12**	**15588**	**11484**	**4430**	**−5.8**	**−6.8**	**−7.9**	**−6.4**	**−7.7**
Std Dev	**156**	**5.2**	**2885**	**4274**	**4816**	**2.9**	**3**	**3.8**	**2.3**	**2.2**
Median	**1864**	**11.9**	**15888**	**11619**	**2687**	**−4.8**	**−5.9**	**−6.1**	**−6.5**	**−6.8**

[nm = not measurable]

doi:10.1371/journal.pone.0083599.t001

Table 2. Characteristics of microcracks embedded within the bone matrix in the control (VOI1) and fatigue-loaded (VOI2) volumes.

	Cr.Dn [#/mm^2]		Cr.Le [μm]		Cr.Dn.Q1 [#/mm^2]		Cr.Le.Q1 [μm]	
Specimens	VOI1	VOI2	VOI1	VOI2	VOI1	VOI2	VOI1	VOI2
#1	3.88	3.03	80.4	68.1	0.73	0.98	35.8	34.8
#2	3.16	2.76	64.1	65.4	0.72	0.6	27.8	34
#3	1.53	1.58	58.4	56.2	0.19	0.41	23.3	25.6
#4	1.97	1.77	69.7	69	0.35	0.53	31.5	31.8
#5	0.9	1.84	76.8	62.9	0.19	0.88	45.2	34.2
#6	3.17	2.84	85.9	70.6	0.67	0.91	38	36.3
#7	2.13	4.14	78.5	57.1	0.38	1.96	41.4	32.6
#8	0.36	0.44	99.5	72.5	0.08	0.18	46.7	42.5
#9	3.23	3.11	77.2	72.9	0.65	0.74	32.2	30.8
#10	2.6	4.59	73.1	95.5	0.43	0.45	31.3	31.6
#11	2.49	2.01	55.4	60.2	0.61	0.41	26.2	27.6
#12	0.23	0.25	51.1	54.4	0.02	0	17.3	-
#13	1.06	1.9	80.4	53.5	0.12	0.33	28.8	24.4
#14	1.08	1.99	66	61.6	0.16	0.61	30.3	27.9
Mean	**1.98**	**2.3**	**72.6**	**65.7**	**0.38**	**0.64**	**32.6**	**31.8**
Std Dev	**1.15**	**1.22**	**13**	**10.8**	**0.26**	**0.47**	**8.2**	**4.9**
Median	**2.05**	**2**	**74.9**	**64.1**	**0.36**	**0.56**	**31.4**	**31.8**

Cr.Dn and Cr.Le correspond to the microcracks density and their average length respectively. Cr.Dn.Q1 and Cr.Le.Q1 corresponds to the microcracks density and the average length of short microcracks, i.e. with length in the first quartile of each sample.

doi:10.1371/journal.pone.0083599.t002

coefficient of variation (standard deviation/mean) was found to be 6.3% for E_{LEBT}.

The mechanical characteristics (Table 1) were found to vary between the specimens. The average initial E_{LEBT} modulus was 15.1±3.0 GPa the average apparent dry density ρ_{dry} was 1792±155 g.mm^{-3} and the average porosity was 12.0±5.2.

No significant trends could be observed between stopping criteria and the other measured variables (nonlinearity or microcracks characteristics).

Ultrasonic (NRUS) measurements

The measurement precision of NRUS, assessed by the coefficient of variation of three measurements with intermediate debonding of the piezo-electric source and repositioning, was found to be 8.5% for α_f. The initial nonlinear values of α_f ranged between −4.3 and −6.2, except for one highly nonlinear specimen ($\alpha_f = -15.5$). The average initial α_f value was −5.8±2.9. After the last damage step (step 1 to 4 depending on the specimen), α_f values ranged between −4.7 and −16.2.

On average, the nonlinear parameter α_f increased with the number of fatigue steps. However, a disparity could be observed between the specimens.

A significant effect of fatigue on α_f was measured for both groups (Group 1: $p<0.05$, no F value due to the number of steps less than four; Group 2, $p = 0.01$, $F = 12.6$). Group 1 including the eight specimens having undergone the first three stages of damage is represented in Fig. 4A. Group 2 including the four specimens having undergone all the four damage steps is represented in Fig. 4B. The result of the post-hoc comparison evidenced statistically significant variations of α_f between damage steps for both groups except between the initial and first step and between the third and last step for specimens of the Group 2.

Finally, note that no correlation was found between the initial nonlinear elastic parameter α_f or its variation $\Delta\alpha_f/\alpha_f$ and the initial elastic modulus E_{LEBT}, the total number of cycles, the apparent density ρ_{dry} nor the sample porosity.

Microtomography

The total number of microcracks found by pooling the data of all the specimens and both VOIs was 4106 with 1380 microcracks leading to the specimen surface and 2726 microcracks fully embedded within the bone volume.

The difference in microdamage characteristics between VOI1 (control region) (Fig. 5A-B) and VOI2 (damage region) (Fig. 5C-D) did not reach statistical significance when all microcracks were included (VOI1: Cr.Le = 71.7±24.0µm; Cr.Dn = 3.11±1.51 #/mm^2 and VOI2: Cr.Le = 69.6±25.7µm; Cr.Dn = 3.33±1.58#/mm^2) nor after excluding from the analysis, microcracks leading to the specimen surface (VOI1: Cr.Le = 72.6±13.0µm; Cr.Dn = 1.98±1.15#/mm^2 and VOI2: Cr.Le = 65.7±10.8µm; Cr.Dn = 2.30±1.22#/mm^2). Damage characteristics of microcracks fully embedded in bone are summarized in Table 2. Note the large inter-specimen variability of Cr.Dn ranging between 0.23#/mm^2 to 3.88#/mm^2 (VOI1) and between 0.25#/mm^2 to 4.59#/mm^2 (VOI2).

In contrast, from the examination of the length distribution of microcracks, it appeared that fatigue cycling resulted in an increase of the density of the shortest microcracks, i.e., those in the first quartile (Q1), whereas the quantity of longer microcracks remained unchanged. The density Cr.Dn.Q1 of the shortest microcracks was significantly different between VOI1 and VOI2, both when all microcracks were included (VOI1: Cr.Dn.Q1 = 0.77±0.38#/mm^2 and VOI2: Cr.Dn.Q1 = 1.06±0.60#/mm^2; $p<0.05$) or when microcracks leading to the surface were excluded (VOI1: Cr.Dn.Q1 = 0.38±0.26#/mm^2 and VOI2: Cr.Dn.Q1 = 0.64±0.47#/mm^2; $p<0.01$) (Fig. 6B). The mean length Cr.Le.Q1 corresponding to the upper limit of the first quartile was found to be 32.6±8.2µm. Such a trend for short microcracks could not be observed for microcracks leading to the specimen surface (Fig. 6A).

The relative variation between VOI2 and VOI1 of density of short microcracks embedded within the bone matrix ΔCr.Dn.Q1/Cr.Dn.Q1 is plotted against the relative variation of the nonlinear parameter $\Delta\alpha_f/\alpha_f$ in Fig. 7. No significant correlation was found taken into account all the specimen (N = 14). However, when the outlier (specimen #6 exhibiting the strongest α_f variation) was

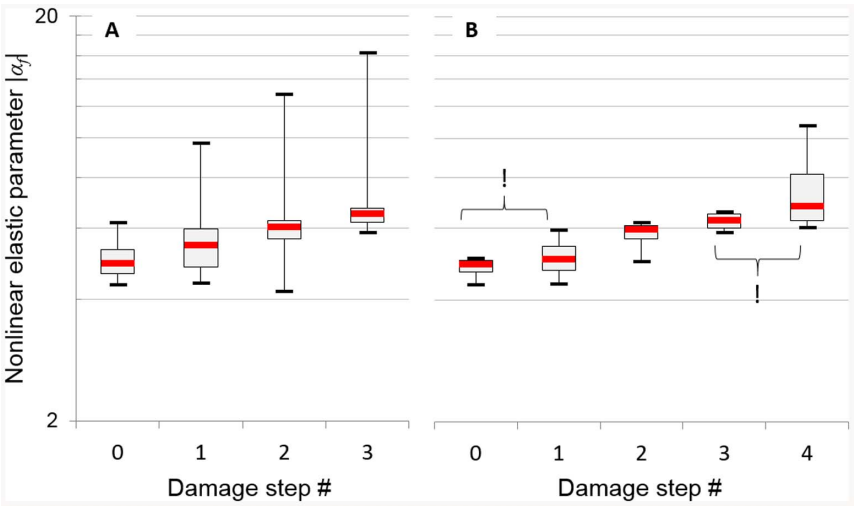

Figure 4. Box plot of the nonlinear elastic parameter α_f after each damage step. (A) Group 1 (N = 8) specimens having undergone the first three stages of damage; (B) Group 2 (N = 4) specimens having undergone the four damage steps. (!) means no significant effect of fatigue on parameter α_f between two steps ($p>0.05$).
doi:10.1371/journal.pone.0083599.g004

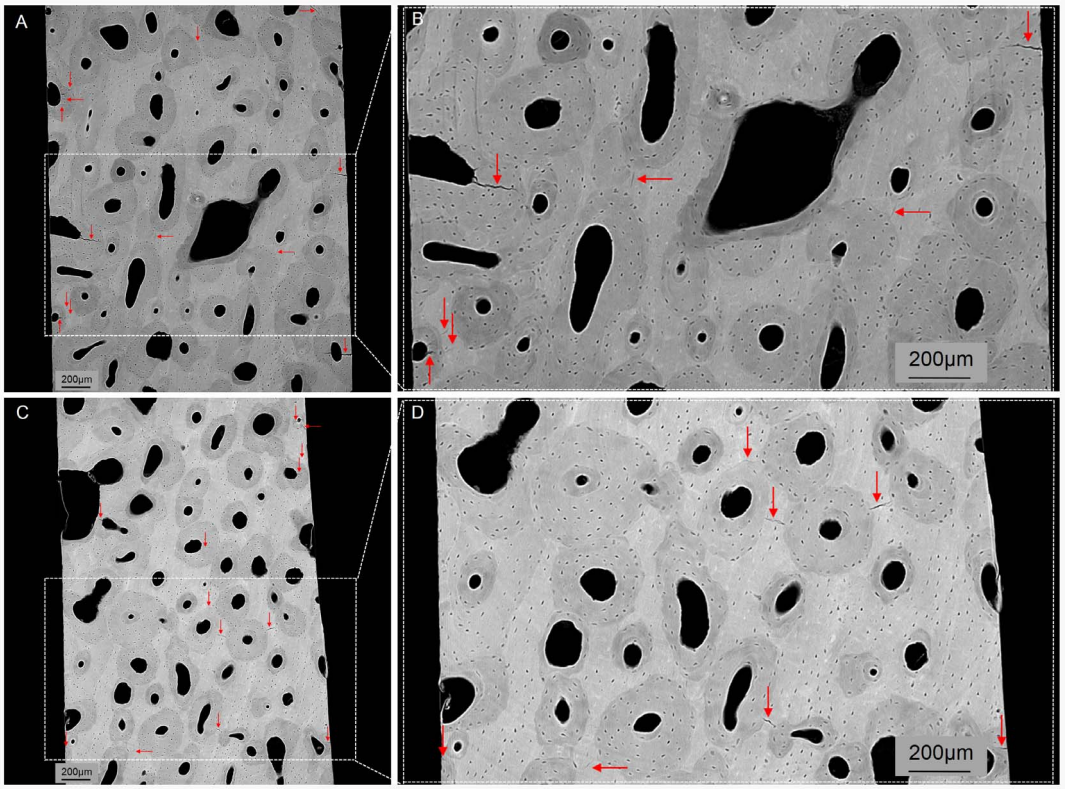

Figure 5. Example of a 2-D transverse cross-section extracted from the (A-B) unloaded region (VOI1) and (C-D) loaded region (VOI2) of the specimen #13. Red arrows point microcracks. Figures B and D are a zoom of the figures A and C respectively.
doi:10.1371/journal.pone.0083599.g005

excluded, a significant correlation of r = 0.6 ($p<0.05$) was found between both quantities.

Discussion

This is the first study reporting the nonlinear elastic hysteretic behavior (assessed by the nonlinear elastic parameter α_f) and microdamage characteristics derived from SR-µCT, concurrently assessed in calibrated human cortical bone specimens during a four point-bending fatigue cycling protocol. By repeating the NRUS measurement protocol after each damage step, we were able to monitor the evolution of the nonlinear behavior during progressively induced mechanical damage, each specimen being its own control. We observed that the damage steps had a statistically significant effect on the nonlinear hysteretic parameter α_f measured by NRUS. This suggests that the parameter α_f is a sensitive marker to bone microdamage induced by *ex vivo* mechanical fatigue test. These results confirm the seminal observations made in previous studies by our group [35–37].

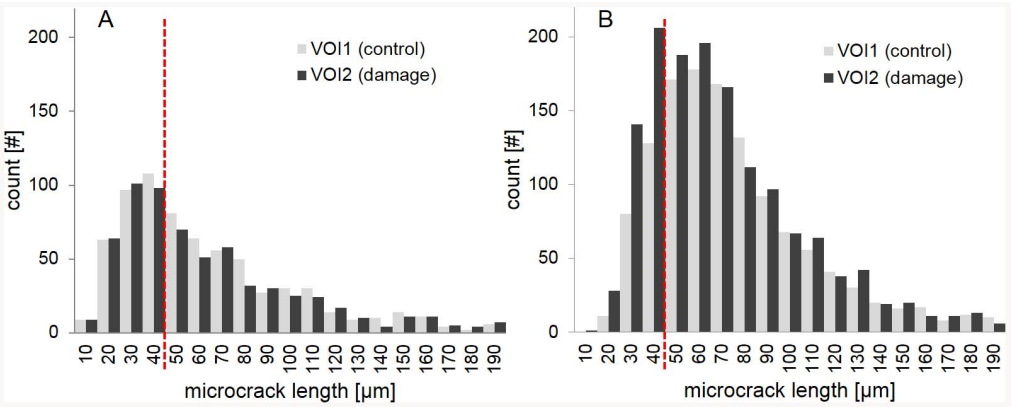

Figure 6. Distribution of microcracks length, in the control zone (VOI1) and the damage zone (VOI2) for all the fourteen specimens. (A) Only microcracks leading to the surface specimen are taken into account; (B) only microcracks fully embedded within the bone matrix are taken into account. In case of microcracks fully embedded within the bone matrix, there is a significant difference (p = 0.01) in the number of microcracks having a length shorter than 40µm between VOI1 and VOI2 in the damage zone.
doi:10.1371/journal.pone.0083599.g006

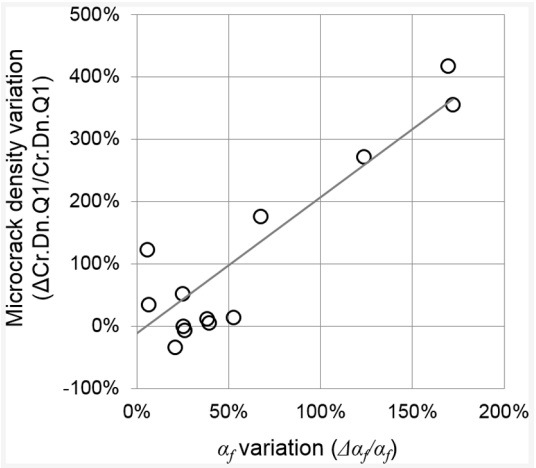

Figure 7. Correlation between the relative variation $\Delta\alpha_f/\alpha_f$ of the nonlinear elastic parameter (α_f represents the difference between the initial value and the value measured after the last damage step) and the relative variation of short microcracks density ΔCr.Dn.Q1/Cr.Dn.Q1 between VOI1 and VOI2. One specimen (#6; ΔCr.Dn.Q1/Cr.Dn.Q1 = 0.36; $\Delta\alpha_f/\alpha_f = 2.48$) exhibiting the strongest α_f variation is not represented
doi:10.1371/journal.pone.0083599.g007

The present study brings a new insight by unraveling the link existing between the nonlinear elastic behavior and some damage characteristics, the latter being derived from μCT volumetric imaging. Our result evidenced that the increase of elastic non linearity was related to an increase of the density of the shortest microcracks embedded within the bone matrix, i.e., those in the first quartile.

Origin of the elastic nonlinearity in bone

The nonlinear hysteretic elasticity (α_f) of human cortical bone samples was measured in this study, allowing the comparison with other materials. Here, the nonlinear hysteretic elasticity typical of damaged materials is measured, as opposed to the classical elastic non linear response which exists in most materials, including undamaged solids, due to intrinsic anharmonicity of, for instance, the crystalline lattice-atomic level vibration.

The initial (pre-fatigue) nonlinear value ($\alpha_f = -5.8 \pm 2.9$) is consistent with the value previously reported for undamaged cortical bovine bone ($\alpha_f = -5.0 \pm 2.5$) [48]. This value is weak (ten times lower than that of intact polycrystal metals [48] or hundred times lower than for rocks [47] but not null, meaning that human cortical bone specimens exhibit low hysteretic elasticity behavior in pre-fatigue (native) configuration. Even after the progressive damage, the nonlinear behavior remains low when compared to other materials.

There are multiple sources of hysteretic nonlinearity in materials. Hysteresis in the dynamic strain-stress relationship is known to be produced by micro-friction, micro-adhesion and clapping due to presence of soft micro-structural features at different scales such as microcracks [56] or dislocations [57]. Such process could be at the origin of the observed pre- and post-damage bone nonlinearities. The sources are not known and were beyond the scope of this study. As bone is a hierarchical material [58], the process could take place at different level of the hierarchical structure:

(i) at the nano-scale level, debonding of collagen fibers [59] could generate nonlinear effect as it is well known in fiber composite materials [34]. Stick-slip friction between collagen fibrils and nanocrystals [60–63] could also be a source of a hysteretic elastic behavior;

(ii) at the micro-scale level, nonlinear behavior could have its origin in the cement line sliding or osteon pull-out [64];

(iii) at the meso-scale level, micro and macrocracks might be the main structure generating nonlinear acoustic phenomena.

This list is not exhaustive but opens up about the multiplicity of factors behind the nonlinear hysteretic elastic behavior of cortical bone. As it stands, we cannot draw any conclusion about the origin of the native (here, "native" means "prior to any damage step") nonlinear behavior of cortical bone. It may have its origin in damage, microcrack or diffuse type, native or induced by sample preparation. Such damage is observed by measuring the control regions located at the ends of the specimens. As for other potential sources of damage (dislocation, delamination, slip osteons, etc.), it would be necessary to assess their magnitude and explore them by dedicated experiments. However, as each sample is its own control, we can attribute unambiguously the increase in the nonlinear hysteretic behavior after fatigue to damage accumulation.

Besides, water saturation, capillarity effects and fluid flow pressure may also play a role as in rocks [65] and concrete [66] by modifying bone nonlinear elasticity, viscoelasticity and relaxation properties. For this reason, a particular attention was given to keep the samples at the same relative humidity (e.g. 15%±5%) during each NRUS experiment.

Pre-existing microdamage (VOI1)

The density of microcracks (Cr.Dn) embedded within undamaged bone volumes ($1.98 \pm 1.15 \#/mm^2$ in VOI1) is one order of magnitude larger compared to the values found in most studies on human cortical femur ($0.21 \pm 0.16 \#/mm^2$ [5], $0.21 \pm 0.21 \#/mm^2$ [15], $0.15 \pm 0.16 \#/mm^2$ [67], $0.1 \pm 0.06 \#/mm^2$ [68]). Only two studies have shown comparable Cr.Dn ranging between $1 \#/mm^2$ to $5 \#/mm^2$ for women older than 45 years old and higher than $1.5 \#/mm^2$ for human femur older than 70 years old [4,6]. However, one has to remind that microcracks density increases with age [2,4–6,67] and that the age of the donors in our study (88.5±9.8) is generally higher than in the above mention studies. This being said, even if we discarded microcracks leading to the surface, we cannot exclude that crack density can be artificially augmented by some artifactual microcracks formed during the preparation process of the specimens, especially those located 500μm from cutting edge [14,53].

Factors other than age of donors and artifactual microcracks, however, can explain the difference between studies. Indeed, microcrack density may depend on the technique used to assess microdamage characteristics [69,70]. For example, the number of microcracks counted by epifluorescence microscopy [70,71] or by backscatter scanning electron (BSE) microscopy [69] could be up to twice the number measured by conventional microscopy based on basic Fuchsin dye. In this study, cortical bone microdamage quantitative assessment was done by SR-μCT. The contrast, resolution and depth of field of SR-μCT images differ from those of conventional optical microscopy-based histomorphometry approaches, which may affect differently the detection of microcracks and their characteristics. A face-to-face comparison between the different techniques would be warranted to provide an answer to this issue.

Induced microdamage (VOI2)

When we considered all the detected microcracks, leading to the surface of the specimens and embedded within the bone matrix, we found no significant change of microcrack density and length. This is at odds with several previous studies, although once again, the difference in technologies used in different studies to quantitatively assess microdamage should be emphasized, namely, X-ray micro-tomography in our study versus optical–based microscopy in previous reports. Several studies report that three or four-point bending fatigue tests on calibrated cortical bone specimens induced the progression of microdamage by increasing microcrack density and length in human [13,15] or bovine bone [12]. However there is no consensus on bone microdamage induced by *in vitro* mechanical fatigue tests. For example, a recent experiment dedicated to four-point bending test on bovine cortical bone, showed no microcrack density variation but only an increase of their average length (control: Cr.Le = 41μm±22μm/loaded: Cr.Le = 108μm±63μm) [51]. In another study on whole canine femur with comparable experimental protocol [72], a modulus loss threshold was observed, i.e. microcracks accumulation started when loading modulus loss exceeds 15%. Moreover, the average microcrack length was not significantly different between control and cyclically loaded specimens, as in the present study. It was suggested that damage initiates at tissue level as nanodamage before being visible as microcracks [72]. However, numerous studies suggest that rather than a continuum between diffuse damage and microcracks, both types of damage are different events. Diffuse damage is generally found to be mainly created in response to tensile stress [12,13] and in young bone [73] whereas microcracking occurs preferentially under compressive stress [15] and in old bone [73].

When the microcracks leading to the specimen surface were analyzed separately, the density of short microcracks was not statistically significantly different between VOI1 (control region) and VOI2 (damage region). This is in contrast with the results obtained when we considered fully embedded microcracks only. The reason for this discrepancy remains unclear. One possibility is that pre-existing and/or preparation microcracks leading to the specimen surface release stress concentration, thus preventing significant growth of microdamage at the periphery of the specimens. On the contrary, microcracking process, as an essential mechanism inside bone specimen to release stress concentration, may explain why small microcracks density increases. Further experiments are required to elucidate this issue.

Microcracking process is well known in fiber-reinforced composite materials as the so-called three-phase modulus degradation curve [74]. The evolution of bone microdamage characteristics (density and length) throughout modulus degradation was observed for the first time in bovine tibia during tension fatigue cycling [14,16]. O'Brien observed that the formation of new microcracks was initiated during an early phase of damage, which confirmed the above mentioned hypothesis. New microcracks grew up to reach a maximal length of about 100μm mainly due to cement lines acting as barriers [75], while only 6% of the native microcrack propagated. Thus, the level of damage depends on the phase of the modulus degradation curve. In early stages of fatigue, damage first manifests by short microcracks, confined to interstitial bone tissue, releasing and redistributing local stress in order to enhance fatigue life, as it was suggested by Sobelman [15].

Our results seem to be in line with the progressive growing of microdamage described in [14,16]. Indeed, we observed a doubling of the shortest microcracks density Cr.Dn.Q1 (those in the first quartile) without an increase of the global microcracks density, neither an expansion of the average length of the pre-existing microcracks. It is likely that our fatigue cycling protocol was not sufficiently strong to increase the average length of the pre-existing microcracks. Nevertheless it was sufficient to lead to the formation of new short microcracks, revealed by the increase of Cr.Dn.Q1. This suggests that the final damage state of our specimens remained low compared to the previous studies [12,13,15,51]

The significant correlation found between the variation of α_f and the variation of Cr.Dn.Q1 is suggestive of the sensibility of the nonlinear hysteretic elastic parameter to newly formed microcracks in early phases of bone damage. However we cannot reject an effect of early diffuse or nanodamage to hysteretic nonlinearity as this damage was not investigated, neither the initiation and growing of a single macrocrack (i.e. known to produce large nonlinear elastic behavior) that was not contained by the microcracking process.

Conclusion

Altogether our results evidence:

i) an increased number of short microcracks in damaged regions compared to the load-free (control) regions. These shortest microcracks, with length in the first quartile, are suspected to be newly formed microcracks as a result of fatigue cycling [14];

ii) a significant effect of damage steps on the nonlinear hysteretic elastic parameter α_f.

iii) a significant relationship between the relative variation of nonlinear elasticity and the relative variation of the density of newly formed microcracks.

The hysteretic nonlinear parameter (α_f) is sensitive to early bone microdamage. Our results suggest that NRUS can be used to monitor fatigue microdamage in *in vitro* experiments. The ability to non invasively quantitatively assess microdamage accumulation in living bones would represent an important step to improve our understanding of skeletal status. However, several scientific and technical problems have to be solved first, such as the adaptation of the nonlinear ultrasound techniques to *in vivo* measurement requirements.

Acknowledgments

The authors are grateful to G Renaud and J Rivière (Laboratoire d'Imagerie Paramétrique, Paris, France) for their helpful comments and suggestions during the preparation of the experiments, as well as to PA Johnson (Los Alamos National Laboratory, NM, USA) for fruitful discussions. The authors acknowledge the support of the ESRF for providing beamtime on beamline ID19 for synchrotron micro-CT imaging in the context of the Long Term Project (LTP) MD431, and to E Boller, M Zuluaga and M Langer for help during the experiments.

Author Contributions

Conceived and designed the experiments: SH SG FP DM PL. Performed the experiments: SH SG FP DM. Analyzed the data: SH SG DM PL. Contributed reagents/materials/analysis tools: SH SG FP DM PL. Wrote the paper: SH PL.

References

1. Frost H (1960) Presence of microscopic cracks in vivo in bone. Henry Ford Hosp Med Bull 8: 35.
2. Diab T, Vashishth D (2007) Morphology, localization and accumulation of in vivo microdamage in human cortical bone. Bone 40: 612–618.
3. Donahue SW, Galley SA (2006) Microdamage in bone: implications for fracture, repair, remodeling, and adaptation. Critical reviews in biomedical engineering 34: 215.
4. Schaffler MB, Choi K, Milgrom C (1995) Aging and matrix microdamage accumulation in human compact bone. Bone 17: 521–525.
5. Norman TL, Wang Z (1997) Microdamage of human cortical bone: Incidence and morphology in long bones. Bone 20: 375–379.
6. Zioupos P (2001) Accumulation of in-vivo fatigue microdamage and its relation to biomechanical properties in ageing human cortical bone. Journal of microscopy 201: 270–278.
7. Taylor D, Hazenberg JG, Lee TC (2007) Living with cracks: Damage and repair in human bone. Nature Materials 6: 263–268.
8. Chapurlat R, Delmas P (2009) Bone microdamage: a clinical perspective. Osteoporosis international 20: 1299–1308.
9. Saito M, Marumo K (2010) Collagen cross-links as a determinant of bone quality: a possible explanation for bone fragility in aging, osteoporosis, and diabetes mellitus. Osteoporosis international 21: 195–214.
10. Allen MR, Burr DB (2011) Bisphosphonate effects on bone turnover, microdamage, and mechanical properties: what we think we know and what we know that we don't know. Bone 49: 56–65.
11. Yeni YN, Fyhrie DP (2002) Fatigue damage-fracture mechanics interaction in cortical bone. Bone 30: 509–514.
12. Diab T, Vashishth D (2005) Effects of damage morphology on cortical bone fragility. Bone 37: 96–102.
13. Boyce TM, Fyhrie DP, Glotkowski MC, Radin EL, Schaffler MB (1998) Damage type and strain mode associations in human compact bone bending fatigue. Journal of Orthopaedic Research 16: 322–329.
14. O'Brien FJ, Taylor D, Lee TC (2003) Microcrack accumulation at different intervals during fatigue testing of compact bone. Journal of Biomechanics 36: 973–980.
15. Sobelman OS, Gibeling JC, Stover SM, Hazelwood SJ, Yeh OC, et al. (2004) Do microcracks decrease or increase fatigue resistance in cortical bone? Journal of Biomechanics 37: 1295–1303.
16. O'Brien FJ, Taylor D, Lee TC (2007) Bone as a composite material: The role of osteons as barriers to crack growth in compact bone. International Journal of Fatigue 29: 1051–1056.
17. Danova NA, Colopy SA, Radtke CL, Kalscheur VL, Markel MD, et al. (2003) Degradation of bone structural properties by accumulation and coalescence of microcracks. Bone 33: 197–205.
18. Martin RB, Yeh OC, Fyhrie DP (2007) On sampling bones for microcracks. Bone 40: 1159–1165.
19. Nalla RK, Kruzic JJ, Kinney JH, Ritchie RO (2005) Aspects of in vitro fatigue in human cortical bone: time and cycle dependent crack growth. Biomaterials 26: 2183–2195.
20. Thurner PJ, Wyss P, Voide R, Stauber M, Stampanoni M, et al. (2006) Time-lapsed investigation of three-dimensional failure and damage accumulation in trabecular bone using synchrotron light. Bone 39: 289–299.
21. Voide R, Schneider P, Stauber M, van Lenthe GH, Stampanoni M, et al. (2011) The importance of murine cortical bone microstructure for microcrack initiation and propagation. Bone 49: 1186–1193.
22. Larrue A, Rattner A, Peter ZA, Olivier C, Laroche N, et al. (2011) Synchrotron Radiation Micro-CT at the Micrometer Scale for the Analysis of the Three-Dimensional Morphology of Microcracks in Human Trabecular Bone. PLoS ONE 6: 21297.
23. Li J, Miller MA, Hutchins GD, Burr DB (2005) Imaging bone microdamage in vivo with positron emission tomography. Bone 37: 819–824. doi:10.1016/j.bone.2005.06.022.
24. Li ZC, Jiang SD, Yan J, Jiang LS, Dai LY (2011) Small-animal PET/CT assessment of bone microdamage in ovariectomized rats. Journal of Nuclear Medicine 52: 769.
25. Nicolella DP, Ni Q, Chan KS (2011) Non-destructive characterization of microdamage in cortical bone using low field pulsed NMR. Journal of the Mechanical Behavior of Biomedical Materials 4: 383–391.
26. Hoff L, Oygarden K, Hagen EK, Falch JA (2003) Diagnosis of osteoporosis using nonlinear ultrasound IEEE, Vol. 1. pp. 1010–1013 Vol. 1.
27. Engan H, Ingebrigtsen K, Oygarden K, Hagen E, Hoff L (2006) Nonlinear Ultrasound Detection of Osteoporosis IEEE. pp. 2096–2099.
28. Laugier P (2008) Instrumentation for in vivo ultrasonic characterization of bone strength. Ultrasonics, Ferroelectrics and Frequency Control, IEEE Transactions on 55: 1179–1196.
29. Bennell K, Hart P, Nattrass C, Wark J (1998) Acute and subacute changes in the ultrasound measurements of the calcaneus following intense exercise. Calcified tissue international 63: 505–509.
30. Nicholson PHF, Bouxsein ML (2000) Quantitative ultrasound does not reflect mechanically induced damage in human cancellous bone. Journal of Bone and Mineral Research 15: 2467–2472.
31. Yeni YN, Shaffer RR, Baker KC, Dong XN, Grimm MJ, et al. (2007) The effect of yield damage on the viscoelastic properties of cortical bone tissue as measured by dynamic mechanical analysis. Journal of Biomedical Materials Research Part A 82A: 530–537.
32. Wynnyckyj C, Willett TL, Omelon S, Wang J, Wang Z, et al. (2011) Changes in bone fatigue resistance due to collagen degradation. Journal of Orthopaedic Research 29: 197–203.
33. Van den Abeele K, Van de Velde K, Carmeliet J (2001) Inferring the degradation of pultruded composites from dynamic nonlinear resonance measurements. Polymer Composites 22: 555–567.
34. Van den Abeele K, Le Bas P, Van Damme B, Katkowski T (2009) Quantification of material nonlinearity in relation to microdamage density using nonlinear reverberation spectroscopy: Experimental and theoretical study. The Journal of the Acoustical Society of America 126: 963.
35. Muller M, Sutin A, Guyer R, Talmant M, Laugier P, et al. (2005) Nonlinear resonant ultrasound spectroscopy (NRUS) applied to damage assessment in bone. Journal of the Acoustical Society of America 118: 3946–3952.
36. Muller M, Tencate JA, Darling TW, Sutin A, Guyer RA, et al. (2006) Microdamage assessment using non-linear resonant ultrasound spectroscopy (NRUS) techniques: A feasibility study. Ultrasonics 44: 245–249.
37. Muller M, Mitton D, Talmant M, Johnson P, Laugier P (2008) Nonlinear ultrasound can detect accumulated damage in human bone. Journal of Biomechanics 41: 1062–1068.
38. Renaud G, Calle S, Remenieras JP, Defontaine M (2008) Non-linear acoustic measurements to assess crack density in trabecular bone. International Journal of Non-Linear Mechanics 43: 194–200.
39. Renaud G, Calle S, Remenieras JP, Defontaine M (2008) Exploration of trabecular bone nonlinear elasticity using time-of-flight modulation. Ieee Transactions on Ultrasonics Ferroelectrics and Frequency Control 55: 1497–1507.
40. Moreschi H, Callé S, Guerard S, Mitton D, Renaud G, et al. (2011) Monitoring trabecular bone microdamage using a dynamic acousto-elastic testing method. Proceedings of the Institution of Mechanical Engineers, Part H: Journal of Engineering in Medicine 225: 1–12.
41. Ulrich TJ, Johnson PA, Muller M, Mitton D, Talmant M, et al. (2007) Application of nonlinear dynamics to monitoring progressive fatigue damage in human cortical bone. Applied Physics Letters 91.
42. Zacharias K, Balabanidou E, Hatzokos I, Rekanos IT, Trochidis A (2009) Microdamage evaluation in human trabecular bone based on nonlinear ultrasound vibro-modulation (NUVM). Journal of Biomechanics 42: 581–586.
43. Van den Abeele K, Carmeliet J, Ten Cate JA, Johnson PA (2000) Nonlinear elastic wave spectroscopy (NEWS) techniques to discern material damage, Part II: Single-mode nonlinear resonance acoustic spectroscopy. Research in Nondestructive Evaluation 12: 31–42.
44. Granke M, Grimal Q, Saïed A, Nauleau P, Peyrin F, et al. (2011) Change in porosity is the major determinant of the variation of cortical bone elasticity at the millimeter scale in aged women. Bone 49: 1020–1026.
45. Currey JD (1988) The effect of porosity and mineral content on the Young's modulus of elasticity of compact bone. Journal of Biomechanics 21: 131–139.
46. Rho JY, Pharr GM (1999) Effects of drying on the mechanical properties of bovine femur measured by nanoindentation. Journal of Materials Science: Materials in Medicine 10: 485–488.
47. Johnson P, Sutin A (2005) Slow dynamics and anomalous nonlinear fast dynamics in diverse solids. Journal of the Acoustical Society of America 117: 124–130.
48. Haupert S, Renaud G, Riviere J, Talmant M, Johnson PA, et al. (2011) High-accuracy acoustic detection of nonclassical component of material nonlinearity. The Journal of the Acoustical Society of America 130: 2654–2661.
49. Griffin LV, Gibeling JC, Gibson VA, Martin RB, Stover SM (1997) Artifactual nonlinearity due to wear grooves and friction in four-point bending experiments of cortical bone. Journal of Biomechanics 30: 185–188.
50. ASTM (2008) Standard Test Method for Flexural Properties of Unreinforced and Reinforced Plastics and Electrical Insulating Materials by Four-Point Bending: D6272.
51. Landrigan M, Roeder R (2009) Systematic error in mechanical measures of damage during four-point bending fatigue of cortical bone. Journal of biomechanics 42: 1212.
52. Meijering E (2010) Neuron Tracing in Perspective. Cytometry Part A 77: 693–704.
53. Arlot ME, Burt-Pichat B, Roux JP, Vashishth D, Bouxsein ML, et al. (2008) Microarchitecture influences microdamage accumulation in human vertebral trabecular bone. Journal of Bone and Mineral Research 23: 1613–1618.
54. Lee TC, Arthur TL, Gibson LJ, Hayes WC (2000) Sequential labelling of microdamage in bone using chelating agents. Journal of Orthopaedic Research 18: 322–325.
55. Lee TC, Mohsin S, Taylor D, Parkesh R, Gunnlaugsson T, et al. (2003) Detecting microdamage in bone. Journal of Anatomy 203: 161–172
56. Guyer RA, Johnson PA (1999) Nonlinear mesoscopic elasticity: Evidence for a new class of materials. Physics Today 52: 30–36.
57. Granato A, Lücke K (1956) Theory of mechanical damping due to disclocations. Journal of Applied Physics 27: 583–593.

58. Weiner S, Wagner HD (1998) The material bone: structure-mechanical function relations. Annual Review of Materials Science 28: 271–298.
59. Ritchie RO, Buehler MJ, Hansma P (2009) Plasticity and toughness in bone. Phys Today 62: 41–47.
60. Gupta HS, Wagermaier W, Zickler GA, Aroush DRB, Funari SS, et al. (2005) Nanoscale deformation mechanisms in bone. Nano Letters 5: 2108–2111.
61. Tai K, Ulm FJ, Ortiz C (2006) Nanogranular origins of the strength of bone. Nano letters 6: 2520–2525.
62. Buehler MJ (2007) Molecular nanomechanics of nascent bone: fibrillar toughening by mineralization. Nanotechnology 18: 295102.
63. Gupta H, Zioupos P (2008) Fracture of bone tissue: The 'hows' and the 'whys'. Medical Engineering & Physics 30: 1209–1226.
64. Behiri J, Bonfield W (1980) Crack velocity dependence of longitudinal fracture in bone. Journal of Materials Science 15: 1841–1849.
65. Van den Abeele K, Carmeliet J, Johnson P, Zinszner B (2002) Influence of water saturation on the nonlinear elastic mesoscopic response in Earth materials and the implications to the mechanism of nonlinearity. J Geophys Res 107: 2121.
66. Payan C, Garnier V, Moysan J (2010) Effect of water saturation and porosity on the nonlinear elastic response of concrete. Cement and Concrete Research 40: 473–476.
67. Wasserman N, Brydges B, Searles S, Akkus O (2008) In vivo linear microcracks of human femoral cortical bone remain parallel to osteons during aging. Bone 43: 856–861.
68. Landrigan MD, Jiliang L, Turnbull TL, Burr DB, Niebur GL, et al. (2011) Contrast-enhanced micro-computed tomography of fatigue microdamage accumulation in human cortical bone. Bone 48: 443–450.
69. Schaffler M, Pitchford W, Choi K, Riddle J (1994) Examination of compact bone microdamage using back-scattered electron microscopy. Bone 15: 483–488.
70. Huja SS, Sayeed Hasan M, Pidaparti R, Turner CH, Garetto LP, et al. (1999) Development of a fluorescent light technique for evaluating microdamage in bone subjected to fatigue loading. Journal of biomechanics 32: 1243–1249.
71. Lee TC, Myers ER, Hayes WC (1998) Fluorescence-aided detection of microdamage in compact bone. Journal of Anatomy 193: 179–184.
72. Burr DB, Turner CH, Naick P, Forwood MR, Ambrosius W, et al. (1998) Does microdamage accumulation affect the mechanical properties of bone? Journal of Biomechanics 31: 337–345.
73. Diab T, Condon KW, Burr DB, Vashishth D (2006) Age-related change in the damage morphology of human cortical bone and its role in bone fragility. Bone 38: 427–431.
74. Reifsnider KL, Jamison R (1982) Fracture of fatigue-loaded composite laminates. International Journal of Fatigue 4: 187–197.
75. Presbitero G, O'Brien F, Clive Lee T, Taylor D (2012) Distribution of microcrack lengths in bone in vivo and in vitro. Journal of Theoretical Biology 304: 164–171.